

Speed of synchronization in complex networks of neural oscillators: Analytic results based on Random Matrix Theory

Marc Timme, Theo Geisel, and Fred Wolf

Max Planck Institute for Dynamics and Self-Organization, and Department of Physics, University of Göttingen, and Bernstein Center for Computational Neuroscience, 37073 Göttingen, Germany

(Received 12 August 2005; accepted 21 November 2005; published online 31 March 2006)

We analyze the dynamics of networks of spiking neural oscillators. First, we present an exact linear stability theory of the synchronous state for networks of arbitrary connectivity. For general neuron rise functions, stability is determined by multiple operators, for which standard analysis is not suitable. We describe a general nonstandard solution to the multioperator problem. Subsequently, we derive a class of neuronal rise functions for which all stability operators become degenerate and standard eigenvalue analysis becomes a suitable tool. Interestingly, this class is found to consist of networks of leaky integrate-and-fire neurons. For random networks of inhibitory integrate-and-fire neurons, we then develop an analytical approach, based on the theory of random matrices, to precisely determine the eigenvalue distributions of the stability operators. This yields the asymptotic relaxation time for perturbations to the synchronous state which provides the characteristic time scale on which neurons can coordinate their activity in such networks. For networks with finite in-degree, i.e., finite number of presynaptic inputs per neuron, we find a speed limit to coordinating spiking activity. Even with arbitrarily strong interaction strengths neurons cannot synchronize faster than at a certain maximal speed determined by the typical in-degree. © 2006 American Institute of Physics. [DOI: 10.1063/1.2150775]

The individual units of many physical systems, from the planets of our solar system to the atoms in a solid, typically interact continuously in time and without significant delay. Thus at every instant of time such a unit is influenced by the current state of its interaction partners. Moreover, particles of many-body systems are often considered to have very simple lattice topology (as in a crystal) or no prescribed topology at all (as in an ideal gas). Many important biological systems are drastically different: their units are interacting by sending and receiving pulses at discrete instances of time. Furthermore, biological systems often exhibit significant delays in the couplings and very complicated topologies of their interaction networks. Examples of such systems include neurons, which interact by stereotyped electrical pulses called action potentials or spikes; crickets, which chirp to communicate acoustically; populations of fireflies that interact by short light pulses. The combination of pulse-coupling, delays, and complicated network topology formally makes the dynamical system to be investigated a high dimensional, heterogeneous nonlinear hybrid system with delays. Here we present an exact analysis of aspects of the dynamics of such networks in the case of simple one-dimensional nonlinear interacting units. These systems are simple models for the collective dynamics of recurrent networks of spiking neurons. After briefly presenting stability results for the synchronous state, we show how to use the theory of random matrices to analytically predict the eigenvalue distribution of stability matrices and thus derive the speed of synchronization in terms of dynamical and network parameters. We find

that networks of neural oscillators typically exhibit speed limits and cannot synchronize faster than a certain bound defined by the network topology.

I. INTRODUCTION

Most neurons in the human central nervous system communicate by sending and receiving brief stereotyped electrical pulses, called action potentials or spikes. Via chemical synaptic connections, these spikes induce changes in the potential across the membrane of the connected postsynaptic neurons.¹ Due to this mode of communication, these neurons interact at discrete instances in time only—and thus behave substantially different from the interacting units of many physical systems. Other important characteristics of neuronal communication are delayed interactions (due to finite propagation speed of the spikes along axons, nonzero time needed for chemical processes across the synapses and signal transmission along the dendrites) and a complex wiring diagram. As in the example of neurons, many networks of interacting units are not arranged in regular lattices. Instead, single units form an intricate network of connections that mediate the interactions. In addition, these connections are often directed, meaning that a connection from one unit to another does not imply a connection in the reverse direction. From a dynamical systems perspective, these aspects—discrete interaction times, interaction delays, and nonsymmetric, complicated wiring diagram—make the theoretical investigation of the exact spiking dynamics of large neural networks a challenging task.

Previous research has occasionally explicitly considered interaction delays in analytical calculations; the complicated topology of neural networks, however, has received much less attention. As a consequence, if one wants to uncover the dynamics beyond numerical investigations, one is often restricted to mean field theoretical arguments or focuses on globally connected networks or on networks of simple local topology.²⁻¹¹

Here we follow the simple and very useful approach of Mirollo and Strogatz¹² to represent the state of a one-dimensional (neural) oscillator not by its membrane potential, but by a phase that encodes the time to the next spike in the absence of any interactions. In the limit of infinitely fast processing of incoming signals (post-synaptic currents), the nonlinear interactions can then be treated analytically in an exact manner. Following some previous reports^{4,13-16} that used the advantages¹⁷ of the Mirollo-Strogatz idea¹² we here present an analytical approach to exactly determine the asymptotic dynamics of spiking neural networks of complicated topology. We particularly focus on how, and how fast, neurons can synchronize their spikes, i.e., coordinate their activity in time in networks of random topology.

The paper is organized as follows. In Sec. II we briefly introduce model networks of pulse-coupled neural oscillators and state the research question. We are interested in the stability of the synchronous state and its asymptotic synchronization properties. Section III gives the details of the derivation of nonlinear stroboscopic maps of perturbed synchronous states in networks of arbitrary connectivity. We explain the emergence of piecewise analytic maps where the pieces are determined by the temporal spiking order of a particular perturbation. This results in a multiple operator nonlinear stability problem. In Sec. IV, we derive first order operators from the stroboscopic maps leading to a stability operator with multiple piecewise linear parts. Since standard eigenvalue analysis is not appropriate for such multiple operator problems, we describe an alternative method to demonstrate stability in Sec. V. Section VI shows how degeneracy can be enforced, i.e., how all multiple linear operators can be made degenerate to one single stability matrix. It turns out that the oscillator rise functions that guarantee degeneracy are of integrate-and-fire type. For this stability problem, standard eigenvalue analysis is suitable. For two ensembles of random networks, we first study their eigenvalue distributions (Sec. VII), analytically predict these distributions by measures derived from Random Matrix Theory (Sec. VIII) and compare the results between numerics and analytics (Sec. IX). In Sec. X, we discuss consequences of the eigenvalue distributions for the speed of synchronization of neural oscillators. We close in Sec. XI, where we summarize the results, discuss some of their consequences and give a brief outlook.

This paper presents new aspects and detailed descriptions of the determination of the asymptotic synchronization time by Random Matrix Theory. Parts of the results on stability and speed limits to network synchronization have been reported in brief in Refs. 15 and 16, respectively. Details of the stability theory, in particular exact eigenvalue bounds and asymptotic stability in the multioperator case, not discussed

here, can be found in Ref. 18. For effects on parameter inhomogeneities, leading to close to synchronous patterns of spikes, we refer the reader to Ref. 19.

II. MODEL OF NEURAL OSCILLATORS

Consider a system of N neural oscillators that interact by sending and receiving pulses via directed connections. The sets $\text{Pre}(i)$ of presynaptic oscillators having input to an oscillator i define the network connectivity. The number of inputs

$$k_i := |\text{Pre}(i)| \quad (1)$$

to every oscillator i , called in-degree in graph theory²⁰ is nonzero, $k_i \geq 1$, and no further restriction on the network topology is imposed unless otherwise stated.

The state of an individual oscillator j is represented by a phaselike variable $\phi_j \in (-\infty, 1]$ that increases uniformly in time,

$$d\phi_j/dt = 1. \quad (2)$$

Upon crossing a firing threshold, $\phi_j(t_f) \geq 1$, at time t_f an oscillator is instantaneously reset to zero, $\phi_j(t_f^+) = 0$, and a pulse is sent. After a delay time τ this pulse is received by all oscillators i connected to j [for which $j \in \text{Pre}(i)$] and induces an instantaneous phase jump

$$\phi_i[(t_f + \tau)^+] = U^{-1}(U(\phi_i[t_f + \tau] + \varepsilon_{ij})). \quad (3)$$

Here, $\varepsilon_{ij} \leq 0$ are the coupling strengths from j to i , which are taken to be purely inhibitory [$\varepsilon_{ij} < 0$ if $j \in \text{Pre}(i)$, $\varepsilon_{ij} = 0$ otherwise] and normalized,

$$\sum_{j=1}^N \varepsilon_{ij} = \varepsilon, \quad (4)$$

throughout this paper.

The rise function U , which mediates the interactions, is monotonic increasing, $U' > 0$, concave (down), $U'' < 0$, and represents the subthreshold dynamics of individual oscillators. This models the dynamics of the membrane potential of a biological neuron that is driven by a current. Note that the function U need to be defined on the entire range of accessible phase values. In particular, inhibitory coupling can lead to negative phase values $\phi_i < 0$.

Large sparsely connected networks of inhibitory neurons were known before to exhibit irregular asynchronous spiking states in which excitatory drive and inhibitory feedback balance out and fluctuation induce spikes.⁵⁻⁷ However, in a previous study¹⁵ we found that regular states, in the homogeneous case defined by exact spike synchrony, coexist with irregular states in these networks at the same parameters (Fig. 1). This means that by external perturbations one can switch between regular and irregular activity. In particular, strong excitatory synchronous inputs can synchronize the network activity. Strong random inputs can switch the network back to the balanced state. If random inputs to the synchronous state are not too strong, the activity relaxes back to the synchronous state. Two major questions intrigued us: (1) Why, given an irregular topology of the network, can the regular synchronous state be stable such that neurons

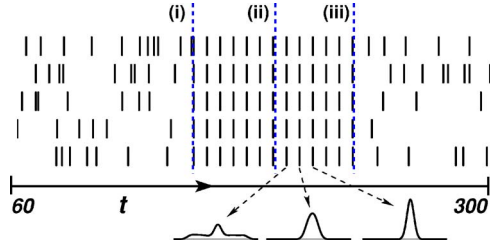


FIG. 1. Irregular, balanced activity coexists with regular, synchronous activity. This enables switching by external stimulus signals. Random network of connection probability $p=0.2$ ($N=400$, $I=4.0$, $\varepsilon=-16.0$, $\tau=0.14$). Firing times of five oscillators are shown in a time window $\Delta t=240$. Vertical dashed lines mark external perturbations. (i) Large excitatory pulses lead to synchronous state, (ii) a small random perturbation ($|\Delta\phi_i| \leq 0.18$) is restored, (iii) a sufficiently large random perturbation ($|\Delta\phi_i| \leq 0.36$) leads to an irregular state. Bottom, time evolution of the spread of the spike times after perturbation (ii), total length $\Delta t=0.25$ each. Decreasing width of the distribution indicates resynchronization. Figure modified from Ref. 15.

resynchronize their spikes upon sufficiently small perturbations? (2) What is the typical time scale for resynchronization, i.e., how fast can neurons coordinate their spiking activity if they are not directly interconnected but interact on large networks of complex topology?

We address these questions analytically in the following, focusing on the speed of synchronization. All results are derived for the simplest of all regular states, the synchronous periodic state, in which all neural oscillators exhibit identical dynamics. However, a similar approach can be used for cluster states in which two or more groups of synchronized oscillators exist,^{4,13} as well as for any periodic solution because they can be traced analytically in the model system used. In the presence of inhomogeneity, the approach needs to be modified but similar principles are expected to apply.

III. NONLINEAR STROBOSCOPIC MAPS: EMERGENCE OF MULTIPLE OPERATORS

The synchronous state

$$\phi_i(t) = \phi_0(t) \quad \text{for all } i, \quad (5)$$

in which all oscillators display identical phases $\phi_0(t)$ on a periodic orbit such that $\phi_0(t+T) = \phi_0(t)$, is one of the simplest states a network of neural oscillators may assume. The normalization of the coupling strengths (4) ensures that it exists but does not tell whether or not it is stable and an attractor of the system. To uncover this, we perform a stability analysis of the synchronous state the period of which is given by

$$T = \tau + 1 - \alpha, \quad (6)$$

where

$$\alpha = U^{-1}(U(\tau) + \varepsilon). \quad (7)$$

For inhibitory coupling ($\varepsilon < 0$) and sufficiently small delay $\tau < 1$ the total input is subthreshold, $U(\tau) + \varepsilon < 1$ such that $\alpha < 1$. A perturbation

$$\delta(0) =: \delta = (\delta_1, \dots, \delta_N) \quad (8)$$

to the phases is defined by

$$\delta_i = \phi_i(0) - \phi_0(0). \quad (9)$$

If we assume that the perturbation is small, in the sense that

$$\max_i \delta_i - \min_i \delta_i < \tau/2 \quad (10)$$

it can be considered to affect the phases of the oscillators at some time just after all signals have been received, i.e., after a time $t > t_0 + \tau$ if all oscillators have fired at $t = t_0$. Such a perturbation will affect the time of the next firing events because the larger the perturbed phase of an oscillator is, the earlier this oscillator reaches threshold and sends a signal.

To construct a stroboscopic period- T map, δ is ordered according to the rank order $\text{rank}(\delta)$ of the δ_i : For each oscillator i we label the perturbations δ_j of its presynaptic oscillators $j \in \text{Pre}(i)$ according to their size

$$\Delta_{i,1} \geq \Delta_{i,2} \geq \dots \geq \Delta_{i,k_i}, \quad (11)$$

where k_i is the number of its presynaptic oscillators (1). The index $n \in \{1, \dots, k_i\}$ counts the signals that arrive successively. Thus, if $j_n \equiv j_n(i) \in \text{Pre}(i)$ labels the presynaptic oscillator from which i receives its n th signal during the period considered, we have

$$\Delta_{i,n} = \delta_{j_n(i)}. \quad (12)$$

In addition, we define

$$\Delta_{i,0} = \delta_i. \quad (13)$$

For illustration, let us consider an oscillator i that has exactly two presynaptic oscillators j and j' such that $\text{Pre}(i) = \{j, j'\}$ and $k_i = 2$ [Figs. 2(a) and 2(d)]. For certain perturbations, oscillator i first receives a signal from oscillator j' and slightly later from oscillator j . This determines the rank order, $\delta_{j'} > \delta_j$, and hence $\Delta_{i,1} = \delta_{j'}$ and $\Delta_{i,2} = \delta_j$ [Fig. 2(a)]. Perturbations with the opposite rank order, $\delta_j > \delta_{j'}$, lead to the opposite labeling, $\Delta_{i,1} = \delta_j$ and $\Delta_{i,2} = \delta_{j'}$ [Fig. 2(d)]. In general, relabeling cannot be achieved by permuting the indices because one oscillator j' may receive an input connection from yet another one m whereas oscillator j may not receive this connection.

We now consider a fixed arbitrary perturbation, the rank order of which determines the $\Delta_{i,n}$ according to the inequalities (11). Using the phase shift function $h(\phi, \varepsilon) = U^{-1}[U(\phi) + \varepsilon]$ and denoting

$$D_{i,n} := \Delta_{i,n-1} - \Delta_{i,n} \quad (14)$$

for $n \in \{1, \dots, k_i\}$ we calculate the time evolution of phase-perturbations δ_i satisfying the bound (10), starting near $\phi_0(0) = \tau/2$ without loss of generality. The stroboscopic time- T map of the perturbations, $\delta_i \mapsto \delta_i(T)$, is obtained from the scheme given in Table I. The time to threshold of oscillator i , which is given in the lower left entry of the scheme,

$$T_i^{(0)} := \frac{\tau}{2} - \Delta_{i,k_i} + 1 - \beta_{i,k_i} \quad (15)$$

is about $\phi_0(0) = \tau/2$ smaller than the period T . Hence the period- T map of the perturbation can be expressed as

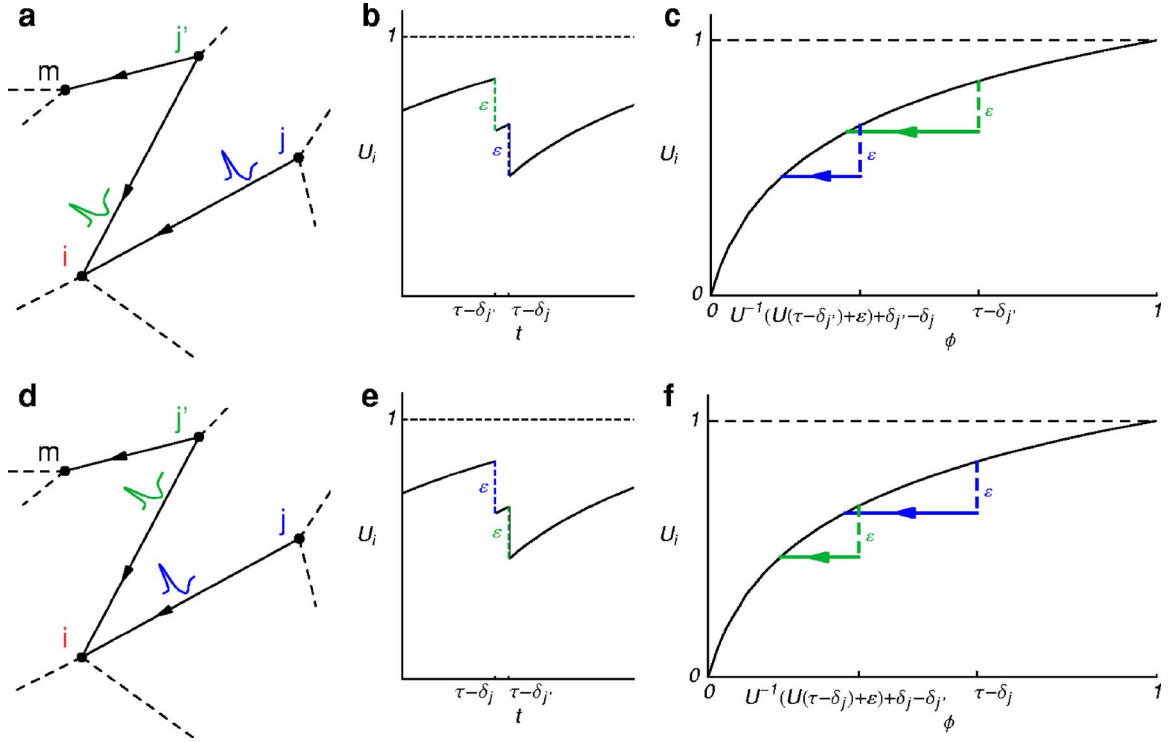


FIG. 2. Two signals arriving almost simultaneously induce different phase changes, depending on their rank order. The figure illustrates a simple case where $\text{Pre}(i) = \{j, j'\}$ and $\delta_i = 0$, (a)–(c) for $\delta_j > \delta_{j'}$ and (d)–(f) for $\delta_j < \delta_{j'}$. (a), (d) Local patch of the network displaying the reception times of signals that are received by oscillator i . Whereas in (a) the signal from j' arrives before the signal of j , the situation in (d) is reversed. (b), (e) Identical coupling strengths induce identical jumps of the potential U but (c), (f) the phase jumps these signals induce are different and depend on the order of the incoming signals. For small $|\delta_i| \ll 1$, individual phase jumps are encoded by the $p_{i,m}$, see (18). The figure displays an example for inhibitory (negative, phase-retarding) coupling but the mechanism generating multiple operators does not depend on the signs of the coupling strengths.

$$\delta_i(T) = T - T_i^{(0)} - \frac{\tau}{2} = \beta_{i,k_i} - \alpha + \Delta_{i,k_i}, \quad (16)$$

where α is given by Eq. (7).

IV. MULTIPLE FIRST ORDER OPERATORS

In order to perform a local stability analysis, we consider the first order approximations of the maps derived in the preceding section. Expanding β_{i,k_i} for small $D_{i,n} \ll 1$ one can prove by induction¹⁸ that

$$\beta_{i,k_i} \doteq \alpha + \sum_{n=1}^{k_i} p_{i,n-1} D_{i,n}, \quad (17)$$

where

$$p_{i,n} := \frac{U' \left[U^{-1} \left(U(\tau) + \sum_{m=1}^n \varepsilon_{ij_m} \right) \right]}{U' \left(U^{-1} \left(U(\tau) + \varepsilon \right) \right)} \quad (18)$$

for $n \in \{0, 1, \dots, k_i\}$ encodes the effect of an individual incoming signal of strength ε_{ij_n} . The statement $x \doteq y$ means that $x = y + \sum_{i,n} \mathcal{O}(D_{i,n}^2)$ as all $D_{i,n} \rightarrow 0$. Substituting the first order approximation Eq. (17) into Eq. (16) using Eq. (14) leads to

$$\delta_i(T) \doteq \sum_{n=1}^{k_i} p_{i,n-1} (\Delta_{i,n-1} - \Delta_{i,n}) + \Delta_{i,k_i} \quad (19)$$

such that after rewriting

$$\delta_i(T) \doteq p_{i,0} \Delta_{i,0} + \sum_{n=1}^{k_i} (p_{i,n} - p_{i,n-1}) \Delta_{i,n} \quad (20)$$

to first order in all $\Delta_{i,n}$. Since $\Delta_{i,n} = \delta_{j_n(i)}$ for $n \in \{1, \dots, k_i\}$ and $\Delta_{i,0} = \delta_i$ according to Eqs. (12) and (13), this results in a first order map

$$\delta(T) \doteq A \delta, \quad (21)$$

where the elements of the matrix A are given by

$$A_{ij} = \begin{cases} p_{i,n} - p_{i,n-1} & \text{if } j = j_n \in \text{Pre}(i), \\ p_{i,0} & \text{if } j = i, \\ 0 & \text{if } j \notin \text{Pre}(i) \cup \{i\}. \end{cases} \quad (22)$$

As for the nonlinear stroboscopic maps (16), because j_n in Eq. (22) identifies the n th pulse received during this period by oscillator i , the first order operator depends on the rank order of the perturbations, $A = A[\text{rank}(\delta)]$. The variables $p_{i,n}$ encode phase jumps evoked by all pulses up to the n th one received. Since the matrix elements (22) are differences of these $p_{i,n}$, matrix elements $A_{i,j}$ and $A_{i,j'}$ with $j \neq j'$ have in general different values depending on the order of incoming signals.

This multioperator problem is induced by the structure of the network together with the pulsed interactions. For networks with homogeneous, global coupling different matrices A can be identified by an appropriate permutation of the oscillator indices. In general, however, this is impossible.

TABLE I. Time evolution of oscillator i in response to k_i successively incoming signals from its presynaptic oscillators j_n , $n \in \{1, \dots, k_i\}$, from which i receives the n th signal during this period. The right-hand column gives the phases $\phi_i(t)$ at times t given in the left-hand column. The time evolution is shown for a part of one period ranging from $\phi_i \approx \tau/2$ to reset, $1 \rightarrow 0$, such that $\phi_i = 0$ in the last row. The first row gives the initial condition $\phi_i(0) = \tau/2 + \delta_i$. The following rows describe the reception of the k_i signals during this period whereby the phases are mapped to $\beta_{i,n}$ after the n th signal has been received. The last row describes the reset at threshold such that the respective time $T_i^{(0)} = \tau/2 - \Delta_{i,k_i} + 1 - \beta_{i,k_i}$ gives the time to threshold of oscillator i .

t	$\phi_i(t)$
0	$\frac{\tau}{2} + \delta_i =: \frac{\tau}{2} + \Delta_{i,0}$
$\frac{\tau}{2} - \Delta_{i,1}$	$h(\tau + D_{i,1}, \varepsilon_{ij_1}) =: \beta_{i,1}$
$\frac{\tau}{2} - \Delta_{i,2}$	$h(\beta_{i,1} + D_{i,2}, \varepsilon_{ij_2}) =: \beta_{i,2}$
\vdots	\vdots
$\frac{\tau}{2} - \Delta_{i,k_i}$	$h(\beta_{i,k_i-1} + D_{i,k_i}, \varepsilon_{ij_{k_i}}) =: \beta_{i,k_i}$
$\frac{\tau}{2} - \Delta_{i,k_i} + 1 - \beta_{i,k_i}$	reset: $1 \rightarrow 0$

Thus even for a network of given number of neuronal oscillators at given connection strengths and given delay and interaction function, the stability of the synchronous state is described by many different operators that depend on the rank order of the perturbation.

V. ALTERNATIVE METHOD TO DETERMINE STABILITY

In most stability problems for periodic orbits in dynamical systems theory, finding the eigenvalues of an appropriate stroboscopic map is sufficient for determining the stability of the orbit. Typically, one eigenvalue equals one and corresponds to perturbation along the periodic orbit trajectory such that there is no restoring force. If all other eigenvalues are smaller than one in absolute value, the periodic orbit is asymptotically stable and all sufficiently close initial states converge to it.

On the contrary, the multioperator property of the stability problem considered here implies that standard eigenvalue analysis fails. However, we found other methods to determine the stability of the synchronous periodic state. We present the results briefly in the following.

To show plain (nonasymptotic) linear stability, observe that the row-sums of the stability matrices are normalized,

$$\sum_{j=1}^N A_{ij} = 1 \quad (23)$$

reflecting the invariance of the periodic orbit with respect to perturbations along it. Given that the coupling strengths are purely inhibitory, $\varepsilon_{ij} \leq 0$, one can show that the $p_{i,n}$ [Eq. (18)] are positive and bounded above by one,

$$0 < p_{i,n} \leq 1, \quad (24)$$

and that they increase with n ,

$$p_{i,n-1} < p_{i,n}. \quad (25)$$

Hence the nonzero off-diagonal elements are positive, $A_{ij_n} = p_{i,n} - p_{i,n-1} > 0$ such that

$$A_{ij} \geq 0 \quad (26)$$

for all $i, j \in \{1, \dots, N\}$. Moreover the diagonal elements

$$A_{ii} = p_{i,0} = \frac{U'(\tau)}{U'(U^{-1}[U(\tau) + \varepsilon])} =: A_0 \quad (27)$$

are identical for all i and satisfy

$$0 < A_0 < 1 \quad (28)$$

because U is monotonically increasing, $U'(\phi) > 0$, and concave down, $U''(\phi) < 0$, for all ϕ . It is important to note that A has the properties Eqs. (23)–(28) independent of the parameters, the network connectivity, and the specific perturbation considered. With these observations, it is straightforward to show that the synchronous state is stable in the sense that small perturbations cannot grow: To first order, a given perturbation $\delta = \delta(0)$ satisfies

$$\|\delta(T)\| := \max_i |\delta_i(T)| \quad (29)$$

$$= \max_i \left| \sum_{j=1}^N A_{ij} \delta_j \right| \quad (30)$$

$$\leq \max_i \sum_j |A_{ij}| |\delta_j| \quad (31)$$

$$\leq \max_i \sum_j |A_{ij}| \max_k |\delta_k| \quad (32)$$

$$= \max_i \sum_j A_{ij} \max_k |\delta_k| \quad (33)$$

$$= \max_k |\delta_k| \quad (34)$$

$$= \|\delta\|, \quad (35)$$

where we use the vector norm

$$\|\delta\| := \max_i |\delta_i|. \quad (36)$$

Thus the length of a perturbation vector does not increase during one period implying that it does not increase for an arbitrary long time. Using methods from graph theory, one can show¹⁸ that for strongly connected networks (in which every oscillator can be reached from every other by following a directed path on the network) the synchronous state is asymptotically stable such that from sufficiently close initial conditions the spiking activity will become exactly synchronous. The results on asymptotic stability use the recurrence properties of strongly connected networks and rely on the fact that every oscillator can communicate with every other at least indirectly. Thus the results for plain and asymptotic

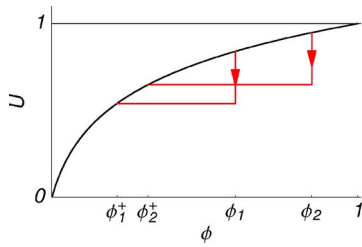


FIG. 3. Intuitive synchronization mechanism: Inhibition synchronizes due to the concavity of U . Simultaneously received inhibitory input decreases phase differences between the receiving oscillators, $|\phi_2(t^*) - \phi_1(t^*)| > |\phi_2(t) - \phi_1(t)|$.

stability are independent of the specific choice of parameters, $\varepsilon_{ij} \leq 0$, $\tau \in (0, 1)$, the potential function $U(\phi)$, and the rank order of the perturbation. They are derived without using the eigenvalues or eigenvectors of a given stability matrix and solve the stability problem exactly. In summary this means that *any* network of the type described above, with normalized inhibitory coupling Eq. (4) exhibits a synchronous state that is at least marginally stable; it is moreover asymptotically stable if the network is strongly connected.

A simple intuitive argument why networks of inhibitorily coupled neural oscillators synchronize can be obtained from the response dynamics of individual units, Fig. 3. If two (or more) neurons simultaneously receive inhibitory input of the same size, their potential is decreased by the same amount such that their potential difference stays unchanged. Due to the negative curvature of the rise function that mediates the negative input, this, however, leads to a decrease of their phase differences, which encode the future spike times. This intuitive explanation holds for simple situations like globally coupled systems with homogeneous coupling strengths. However, the synchronization dynamics is more complicated if the inputs are not of equal size or only one input exists for some unit, as, e.g., in a directed ring of neurons.

In the case of integrate and fire functions $U = U_{\text{IF}}$ one can derive¹⁸ stability results based on the eigensystem because all stability operators become degenerate; see below for details of the degeneracy for networks of integrate and fire neurons. The Geršgorin disk theorem then bounds all eigenvalues in a disk of radius $r_G = 1 - A_0$ centered at A_0 , touching the unit circle from the inside at $z = 1$. It ensures that the eigenvalue largest in magnitude is $\lambda_1 = 1$, with corresponding eigenvector $\mathbf{v}_1 \propto (1, 1, \dots, 1)^T$. For strongly connected networks, the Perron Frobenius theorem implies that this eigenvalue is unique, i.e., all other eigenvalues are smaller than one in absolute value. Thus all perturbations that contain components other than \mathbf{v}_1 will decay towards a uniform perturbation. Such an analysis confirms that networks of arbitrary connectivity are at least marginally stable and strongly connected networks exhibit asymptotically stable synchronous states, as shown above by alternative methods.

If networks consist of several strongly connected components, the analysis is much more involved and structural identification of strongly connected components and the wiring among them is required. Such networks display a kind of nonsynchronous activity that is controlled by the coarse and

fine scale structure of the network, cf. Ref. 21. This state seems to be universal among networks of coupled oscillators exhibiting a synchronization mechanism.

VI. ENFORCING DEGENERACY: THE PHOENIX INTEGRATE-AND-FIRE

From the general class of concave increasing rise functions, we now derive a subclass of rise functions in which all multiple operators degenerate to a single stability matrix if the coupling strength are suitably chosen. Interestingly, it turns out that the class of standard leaky integrate-and-fire oscillators provides potential functions consistent with this condition.

A general potential function U that is monotonically increasing, $U'(\phi) > 0$, and concave (down), $U''(\phi) < 0$, yielded stability operators A in the first order map (21) that are defined by their respective matrix elements (22) in terms of differences of the $p_{i,n}$ [Eq. (18)] that in turn describe the effect of the n th signal received by oscillator i within the period considered. Thus, the actual stability operator to be used for a specific perturbation depends on the rank order of the incoming signals given this perturbation. Can the multiple linear operators be made degenerate? If so, the eigensystem of the resulting matrix completely describes the asymptotic synchronization dynamics.

Consider a network for which the coupling strengths of all presynaptic oscillators $j \in \text{Pre}(i)$ are identical,

$$\varepsilon_{ij} = \frac{\varepsilon}{k_i} \quad (37)$$

for each oscillator i . For such a network, two matrix elements are interchanged at the boundary of the domains of definition of an individual operator. For instance, assume that an oscillator i has exactly two presynaptic oscillators j and j' . If a perturbation is changed such that $\delta_j > \delta_{j'}$ is turned into $\delta_j < \delta_{j'}$, the operator A will change from $A = A^{(1)}$ to $A = A^{(2)}$ where the nonzero off-diagonal elements of row i read

$$A_{ij}^{(1)} = A_{ij_1} = p_{i,1} - p_{i,0}, \quad A_{ij'}^{(1)} = A_{ij_2} = p_{i,2} - p_{i,1}, \quad (38)$$

$$A_{ij}^{(2)} = A_{ij_2} = p_{i,2} - p_{i,1}, \quad A_{ij'}^{(2)} = A_{ij_1} = p_{i,1} - p_{i,0}, \quad (39)$$

respectively. As above, j_1 labels the oscillator presynaptic to i that has sent the first signal to i during the period considered, and j_2 labels the presynaptic oscillator that has sent the second one such that

$$j_1 = j \text{ and } j_2 = j' \Leftrightarrow \delta_j > \delta_{j'}, \quad (40)$$

$$j_1 = j' \text{ and } j_2 = j \Leftrightarrow \delta_{j'} > \delta_j. \quad (41)$$

Degeneracy of these two, in general distinct, cases requires that

$$A_{ij}^{(k)} = A_{ij}^{(l)} \quad (42)$$

for $k, l \in \{1, 2\}$ or, equivalently,

$$p_{i,2} - p_{i,1} = p_{i,1} - p_{i,0}. \quad (43)$$

If every oscillator $i \in \{1, \dots, N\}$ in the network has k_i presynaptic oscillators, the degeneracy condition is easily generalized to Eq. (42) with k and l running over all different stability matrices that occur for all possible differently ordered perturbations. Expressed in terms of the $p_{i,n}$, which describe the effect of individual incoming pulses, we obtain

$$p_{i,n} - p_{i,n-1} = p_{i,m} - p_{i,m-1} \quad (44)$$

for all $i \in \{1, \dots, N\}$ and all $n, m \in \{1, \dots, k_i\}$.

If we define

$$q(x_{i,n}) := p_{i,n} = \frac{U'(U^{-1}[U(\tau) + x_{i,n}])}{U'(U^{-1}[U(\tau) + \varepsilon])}, \quad (45)$$

where

$$x_{i,n} = \sum_{m=1}^n \varepsilon_{ij_m} = \frac{n\varepsilon}{k_i} \quad (46)$$

for $n \leq k_i$, the requirement (44) is satisfied if

$$q'(x) = \text{const} \quad (47)$$

in the relevant interval $x \in [\varepsilon, 0]$. Note that $\varepsilon < 0$ because we consider inhibitory coupling. The first derivative of $q(x)$ satisfies

$$q'(x) \propto \frac{U''(U^{-1}[U(\tau) + x])}{U'(U^{-1}[U(\tau) + x])} =: \frac{U''(h(x))}{U'(h(x))}, \quad (48)$$

where $h(x) = U^{-1}[U(\tau) + x]$ is an invertible function of x . Together with Eq. (47) this leads to a differential equation

$$U'' = cU', \quad (49)$$

where $c \in \mathbb{R}$ is a constant. The solution $U(\phi) = a + be^{c\phi}$ with constants $a, b, c \in \mathbb{R}$ together with the normalization $U(0) = 0$, $U(1) = 1$, and the monotonicity and concavity requirements, $U'(\phi) > 0$ and $U''(\phi) < 0$, yield the one-parameter family of solutions in integrate-and-fire form

$$U(\phi) = U_{\text{IF}}(\phi) = I(1 - e^{-\phi T_{\text{IF}}}), \quad (50)$$

where $I > 1$ and $T_{\text{IF}} = \ln[I/(I-1)] > 0$. This leads to

$$U'_{\text{IF}}(\phi) = IT_{\text{IF}} e^{-\phi T_{\text{IF}}}, \quad (51)$$

$$U_{\text{IF}}^{-1}(y) = \frac{1}{T_{\text{IF}}} \ln \left(1 - \frac{y}{I} \right)^{-1}, \quad (52)$$

and

$$U_{\text{IF}}^{-1}[U_{\text{IF}}(\phi) + \varepsilon] = \frac{1}{T_{\text{IF}}} \ln \left(e^{-\phi T_{\text{IF}}} - \frac{\varepsilon}{I} \right)^{-1} \quad (53)$$

such that

$$U'_{\text{IF}}(U_{\text{IF}}^{-1}[U(\phi) + \varepsilon]) = T_{\text{IF}} (I e^{-\phi T_{\text{IF}}} - \varepsilon) \quad (54)$$

and

$$p_{i,n} = \frac{U'_{\text{IF}}(U_{\text{IF}}^{-1}[U_{\text{IF}}(\tau) + \sum_{m=1}^n \varepsilon_{ij_m}])}{U'_{\text{IF}}(U_{\text{IF}}^{-1}[U_{\text{IF}}(\tau) + \varepsilon])} \quad (55)$$

$$= \frac{I e^{-\tau T_{\text{IF}}} - \sum_{m=1}^n \varepsilon_{ij_m}}{I e^{-\tau T_{\text{IF}}} - \varepsilon}. \quad (56)$$

Thus, by construction, if we substitute $\varepsilon_{ij_n} = \varepsilon/k_i$ all nonzero off-diagonal elements

$$A_{ij_n} = p_{i,n} - p_{i,n-1} = \frac{1}{I e^{-\tau T_{\text{IF}}} - \varepsilon} \frac{\varepsilon}{k_i} \quad (57)$$

in one row i of the stability matrix are identical,

$$A_{ij_n} = A_{ij_m}, \quad (58)$$

for all $n, m \in \{1, \dots, k_i\}$.

One should note that, given the coupling strengths satisfy Eq. (37), the condition (47) is sufficient but not necessary for degeneracy of all operators. At given parameters and a given network connectivity, one can construct potential functions that fulfill condition (47) only on (local) average such that the requirement for identical (nonzero) off-diagonal matrix elements in each row (44) is still satisfied. If we do not *a priori* fix the parameters and the network structure, however, the potential function U_{IF} uniquely leads to operator degeneracy within the class of concave down, increasing functions.

This degeneracy has important consequences. Whereas for the multioperator problem the dynamics in the vicinity of the synchronous state is determined by an (unknown but deterministic) sequence of different linear operators, the dynamics in case of degeneracy is typically determined by the eigenvectors and eigenvalues of a single matrix A . In particular, the second largest eigenvalue

$$\lambda_m := \max\{|\lambda_i| : |\lambda_i| < 1\} \quad (59)$$

of this matrix A determines the asymptotic speed of convergence towards the synchronous state,

$$|\delta(n+l)T| \sim \lambda_m^n |\delta(l)T| \quad (60)$$

for $n, l \gg 1$.

Interestingly, the derivation of a condition for degeneracy led to the standard leaky integrate-and-fire model as a subclass of models that imply degeneracy for suitably chosen coupling strengths. Starting from this degenerate case of operators now enables us to develop a characterization of the synchronization dynamics in terms of eigenvalues of that operator.

VII. LOCATION OF EIGENVALUES IN LARGE RANDOM NETWORKS

How fast do random networks synchronize? The characteristic asymptotic time of synchronization, $\tau_{\text{syn}} = -1/\ln(\lambda_m)$, see Eq. (93) below, is given in terms of the second largest eigenvalue λ_m that we determine from the distribution of eigenvalues in the following sections. In this section, we present examples for the distribution of eigenvalues of stability matrices describing the asymptotic dynamics of large asymmetric random networks of integrate-and-fire oscillators

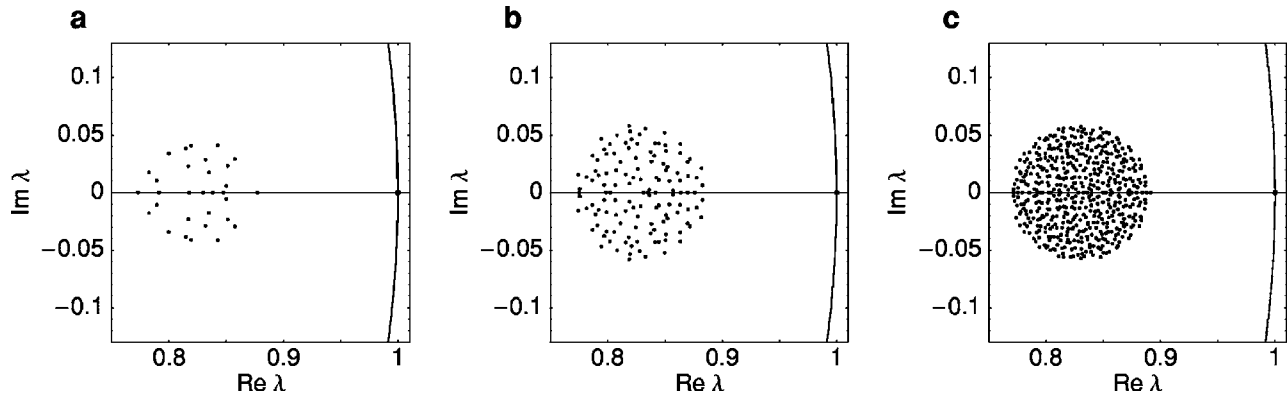


FIG. 4. Distribution of eigenvalues λ_i in the complex plane for networks of fixed in-degree $k=8$ and different sizes (a) $N=32$, (b) $N=128$, (c) $N=512$. For large networks, the nontrivial eigenvalues seem to be distributed uniformly on a disk in the complex plane. The arc through the trivial eigenvalue (dot at $z=\lambda_1=1$) is a sector of the unit circle. Parameters of integrate-and-fire oscillators are $I=1.1$, $\varepsilon=-0.2$, $\tau=0.05$.

in the vicinity of the synchronous state. From the details of the analysis described above, we know that all eigenvalues must be located in a Geršgorin disk K in the complex plane that is centered at $A_0 < 1$ [Eq. (28)] and has radius $1 - A_0$ such that it contacts the unit circle at $z=1$ from the inside. In the following, we consider neural oscillators that interact inhibitory on two classes of random networks (defined in Secs. VII A and VII B). The potential functions of the oscillators are of the integrate-and-fire form $U(\phi) = U_{\text{IF}}(\phi) = I(1 - e^{-\phi T_{\text{IF}}})$, where $T_{\text{IF}} = \ln(I/(I-1))$. The nonzero coupling strength are chosen according to $\varepsilon_{ij} = \varepsilon/k_i$. We consider only sparsely connected networks which lead to sparse stability matrices where we term a matrix “sparse” if at least a positive fraction of its entries is zero in the limit of large N .

A. Networks with constant in-degree

The first class of networks is given by random networks in which all oscillators i have the same number $k_i=k$ of presynaptic oscillators which are independently drawn from the set of all other oscillators with uniform probability. When increasing the network size N , the number of connections k per oscillator is kept fixed. We numerically determined the eigenvalues of different stability matrices changing the network size $N \in \{2^6, \dots, 2^{14}\}$, the in-degree $k \in \{2, \dots, 2^8\}$, and the dynamical parameters ε , τ , and I such that $A_0 \in [0.6, 0.9]$. In general, we find that, for sufficiently large N and sufficiently large k , the nontrivial eigenvalues resemble a disk in the complex plane that is centered at about A_0 but has a radius r that is smaller than the upper bound given by the Geršgorin theorem,

$$r < 1 - A_0. \quad (61)$$

Note that, due to the invariance of the periodic orbit with respect to globally constant phase shifts, there is always a trivial eigenvalue $\lambda_1=1$. As an example, the eigenvalue distributions in the complex plane are displayed in Fig. 4 for specific parameters and differently sized networks.

B. Networks with constant connection probability

The second class of networks is given by random networks for which every connection between any oscillator i

and any other oscillator $j \neq i$ is present with given probability p . When increasing N , this probability is kept fixed such that the number of connections per oscillator is proportional to N . As for the other class of random networks, we find numerically that the distribution of nontrivial eigenvalues resemble disks in the complex plane that are smaller than the Geršgorin disk (61) but centered at about the same point A_0 . We numerically determined the distribution of eigenvalues for $N \in \{2^8, \dots, 2^{14}\}$, $p \in [0.01, 0.2]$, and the dynamical parameters ε , τ , and I such that $A_0 \in [0.6, 0.9]$. Figure 5 displays examples of eigenvalue distributions for differently sized networks at otherwise identical parameters.

VIII. PREDICTIONS FROM RANDOM MATRIX THEORY

The results of the preceding section indicate that the eigenvalues of stability matrices for large asymmetric random networks of integrate-and-fire oscillators are located in disks in the complex plane if the network size N is sufficiently large. If this could be demonstrated independent of specific parameters, it would be guaranteed that all nontrivial eigenvalues are separated from the unit circle. Thus the main condition required for the robustness of the stable synchronous state under a structural perturbation to the dynamics of the system would be satisfied. Moreover, the asymptotic synchronization time can be predicted analytically from these results.

How can we predict the location of the eigenvalues? Since we are considering random networks, a natural starting point is the theory of random matrices. Random Matrix Theory has been investigated intensively since the early 1950s (Ref. 22) (see also Refs. 23 and 24) and turned out to be a valuable tool for both qualitative and quantitative description of spectral properties of complex systems. For instance, it describes level correlations in nuclear physics²⁵ as well as quantum mechanical aspects of chaos.^{26,27} In applications of Random Matrix Theory to physical problems, it is generally assumed that the details of the physical system are less important for many statistical properties of interest. Often it turns out that important statistical properties such as the distribution of spacings of energy levels in quantum systems are well described by the respective properties of ran-

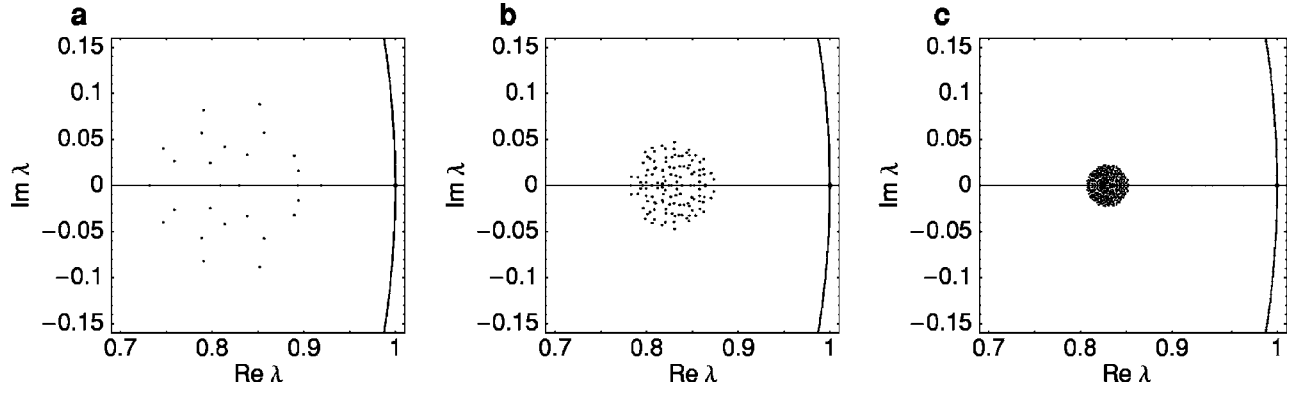


FIG. 5. Distribution of eigenvalues λ_i in the complex plane for networks of fixed connection probability $p=0.1$ and different sizes (a) $N=32$, (b) $N=128$, (c) $N=512$. For large networks, the nontrivial eigenvalues seem to be distributed uniformly on a disk in the complex plane, the radius of which shrinks with increasing network size. The arc through the trivial eigenvalue (dot at $z=\lambda_1=1$) is a sector of the unit circle. Parameters of integrate-and-fire oscillators are $I=1.1$, $\varepsilon=-0.2$, $\tau=0.05$.

dom matrices that respect the same symmetries as the physical system. Both theoretical investigations and applications of Random Matrix Theory have focused on symmetric matrices. Asymmetric matrices are less well understood²⁸ and found only limited applicability. In the following, we will evaluate the applicability of Random Matrix Theory for estimating distributions of eigenvalues of asymmetric stability matrices.

A. Ensembles of symmetric and asymmetric random matrices

For the case of real *symmetric* random $N \times N$ matrices $J=J^T$ with independent, identically distributed components $J_{ij}=J_{ji}$, it is believed^{29,30} that there are exactly two universality classes. Every ensemble of matrices within one of these universality classes exhibits the same distribution of eigenvalues in the limit of large matrices, $N \rightarrow \infty$, but the eigenvalue distributions are in general different for the two classes. Both universality classes are characterized by specific ensembles of matrices the elements of which are distributed according to a simple probability distribution. The class of sparse matrices is represented by the probability distribution

$$p_{\text{sparse}}(J_{ij}) = \frac{k}{N} \delta\left(J_{ij} - \frac{1}{k}\right) + \left(1 - \frac{k}{N}\right) \delta(J_{ij}), \quad (62)$$

where k is the (finite) average number of entries in any row i and $\delta(\cdot)$ is the Dirac delta distribution. The class of Gaussian random matrices is exemplified by a Gaussian distribution of matrix elements

$$p_{\text{Gauss}}(J_{ij}) = N^{1/2} (2\pi s^2)^{-(1/2)} \exp\left(-\frac{NJ_{ij}^2}{2s^2}\right). \quad (63)$$

To obtain symmetric matrices, one chooses $J_{ij}=J_{ji}$ and $J_{ii}=0$ for both ensembles. Thus the arithmetic mean of the eigenvalues is zero,

$$[\lambda_i]_i := \frac{1}{N} \sum_{i=1}^N \lambda_i = \frac{1}{N} \sum_{i=1}^N J_{ii} = 0 \quad (64)$$

and the ensemble variance of the matrix elements scale like

$$\sigma^2 = \langle J_{ij}^2 \rangle = \frac{r^2}{N} \quad (65)$$

for $N \gg 1$. For the Gaussian symmetric ensemble, it is known^{22,24} that the distribution of eigenvalues $\rho_{\text{Gauss}}^s(\lambda)$ in the limit $N \rightarrow \infty$ is given by Wigner's semicircle law

$$\rho_{\text{Gauss}}^s(\lambda) = \begin{cases} \frac{1}{2\pi r^2} (4r^2 - \lambda^2)^{1/2} & \text{if } |\lambda| \leq 2r, \\ 0 & \text{otherwise.} \end{cases} \quad (66)$$

The ensemble of sparse matrices²⁹⁻³² exhibits a different eigenvalue distribution $\rho_{\text{sparse}}^s(\lambda)$ that depends on the finite number k of nonzero entries per row and approaches the distribution $\rho_{\text{Gauss}}^s(\lambda)$ in the limit of large k such that

$$\lim_{k \rightarrow \infty} \rho_{\text{sparse}}^s(\lambda) = \rho_{\text{Gauss}}^s(\lambda). \quad (67)$$

It is important to note that in the limit of large N the distributions ρ_{sparse}^s and ρ_{Gauss}^s eigenvalues depend only on the one parameter r , that is derived from the variance of the matrix elements (65).

For real, *asymmetric* matrices (independent J_{ij} and J_{ji}), there are no analytical results for the case of sparse matrices but only for the case of Gaussian random matrices. The Gaussian asymmetric ensemble [e.g., Eq. (63) with independent J_{ij} and J_{ji}] yields the distribution of complex eigenvalues in a disk in the complex plane^{33,34}

$$\rho_{\text{Gauss}}^a(\lambda) = \begin{cases} (\pi r^2)^{-1} & \text{if } |\lambda| \leq r, \\ 0 & \text{otherwise,} \end{cases} \quad (68)$$

where r from Eq. (65) is the radius of the disk that is centered at zero. Like in the case of symmetric matrices, this distribution also depends only on one parameter r , that is derived from the variance of the matrix elements.

B. Stability matrices and the Gaussian asymmetric ensemble

In the numerical studies of stability matrices for random networks (Sec. VII), we observed that all nontrivial eigenvalues of sparse stability matrices A are located on or near a disk in the complex plane (Figs. 4 and 5). Since this is also

predicted by the theory of asymmetric Gaussian random matrices, let us compare these predictions to numerical results. If the distribution of eigenvalues of sparse asymmetric random matrices ρ_{sparse}^a for $k \gg 1$ is approximately equal to the distribution of Gaussian asymmetric matrices, $\rho_{\text{sparse}}^a(\lambda) \approx \rho_{\text{Gauss}}^a(\lambda)$, in analogy to the case of symmetric matrices (67), and Random Matrix Theory is applicable to the stability matrices at all, we can obtain an analytical prediction for the radii of the disks of eigenvalues.

The elements of the original stability matrix A have an average

$$[A_{ij}] = \frac{1}{N} \sum_{j=1}^N A_{ij} = \frac{1}{N} \quad (69)$$

and a second moment

$$[A_{ij}^2] = \frac{1}{N} \sum_{j=1}^N A_{ij}^2 = \frac{1}{N} \left(A_0^2 + \sum_{\substack{j=1 \\ j \neq i}}^N A_{ij}^2 \right), \quad (70)$$

where the off-diagonal sum is bounded above and below by

$$\frac{(1-A_0)^2}{\max_i k_i} \leq \sum_{\substack{j=1 \\ j \neq i}}^N A_{ij}^2 \leq (1-A_0)^2 \quad (71)$$

due to the normalization (23).

The variance $\sigma_A^2 = [A_{ij}^2] - [A_{ij}]^2$ given by

$$\sigma_A^2 = \frac{A_0^2}{N} + \frac{\sum_{j \neq i} A_{ij}^2}{N} - \frac{1}{N^2} \quad (72)$$

is thus also bounded

$$\frac{A_0^2}{N} + \frac{(1-A_0)^2}{N(N-1)} - \frac{1}{N^2} \leq \sigma_A^2 \leq \frac{A_0^2 + (1-A_0)^2}{N} - \frac{1}{N^2} \quad (73)$$

because $\max_i k_i \leq N-1$. The eigenvalues of the original matrix A have the average value

$$[\lambda_i] := \frac{1}{N} \sum_{i=1}^N \lambda_i = \frac{1}{N} \sum_{i=1}^N A_{ii} = A_0. \quad (74)$$

To directly compare the ensemble of the stability matrices considered here to random matrices with zero average eigenvalue, $\langle \lambda_i \rangle = 0$, and given variance (65), we transform the stability matrix A to

$$A'_{ij} = A_{ij} - A_0 \delta_{ij} \quad (75)$$

for $i \in \{1, \dots, N\}$. Here δ_{ij} denotes the Kronecker delta, $\delta_{ij} = 1$ if $i=j$ and $\delta_{ij} = 0$ if $i \neq j$. The transformation to A' shifts all eigenvalues by $-A_0$ and hence the average value of the eigenvalues to

$$[\lambda'_i] = 0. \quad (76)$$

In addition

$$[A'_{ij}] = [A_{ij}] - \frac{A_0}{N} = \frac{(1-A_0)}{N} \quad (77)$$

and

$$[A'_{ij}{}^2] = [A_{ij}^2] - \frac{A_0^2}{N} \quad (78)$$

such that the variance is

$$\sigma_{A'}^2 = \sigma_A^2 - \frac{A_0^2}{N} + \frac{2A_0}{N^2} - \frac{A_0^2}{N^2} \quad (79)$$

$$= \frac{1}{N} \left(\sum_{\substack{j=1 \\ j \neq i}}^N A_{ij}^2 - \frac{(1-A_0)^2}{N} \right). \quad (80)$$

The eigenvalue distribution of this ensemble of rescaled stability matrices A' for random networks may be compared to the Gaussian asymmetric ensemble with zero average eigenvalue and variance $\sigma_{A'}^2$. In such a comparison, the additional eigenvalue $\lambda_1 = 1$ of A , is neglected. This should not matter for large networks ($N \gg 1$).

It is important to note that we compare the location of eigenvalues of a *sparse* matrix with deterministic nonzero entries at certain random positions with the eigenvalue distribution of the *Gaussian* ensemble, which consists of fully occupied matrices with purely random entries.

If we assume that the eigenvalue distributions for these two ensembles of networks with fixed in-degree and networks with a fixed connection probability are similar to those for random Gaussian matrices, we obtain a prediction

$$r^2 \approx N \sigma_{A'}^2 \quad (81)$$

for the radius of the disk of eigenvalues from Eq. (65). For further investigations, we consider the two exemplary classes of large random networks of integrate-and-fire oscillators discussed in Sec. VII. If we assume that the stability matrix A has exactly k nonzero off-diagonal elements per row and identical coupling strength $\varepsilon_{ij} = \varepsilon/k$ between connected integrate-and-fire oscillators, the off-diagonal sum is exactly equal to

$$\sum_{n=1}^k A_{ij_n}^2 = \frac{(1-A_0)^2}{k}, \quad (82)$$

such that the variance of A equals

$$\sigma_A^2 = \frac{A_0^2}{N} + \frac{(1-A_0)^2}{Nk} - \frac{1}{N^2} \quad (83)$$

and the variance of A' is given by

$$\sigma_{A'}^2 = \frac{1}{N} (1-A_0)^2 \left(\frac{1}{k} - \frac{1}{N} \right). \quad (84)$$

If we now take the prediction from Random Matrix Theory r_{RMT} for the radius r of the disk of eigenvalues of the stability matrices, we obtain

$$r_{\text{RMT}} = N^{1/2} \sigma_{A'} = (1-A_0) \left(\frac{1}{k} - \frac{1}{N} \right)^{1/2}. \quad (85)$$

In random networks where all oscillators have exactly k presynaptic oscillators, the approximation for the variance of A (and thus of A') is exact. If the random network is constructed by choosing every connection independently with

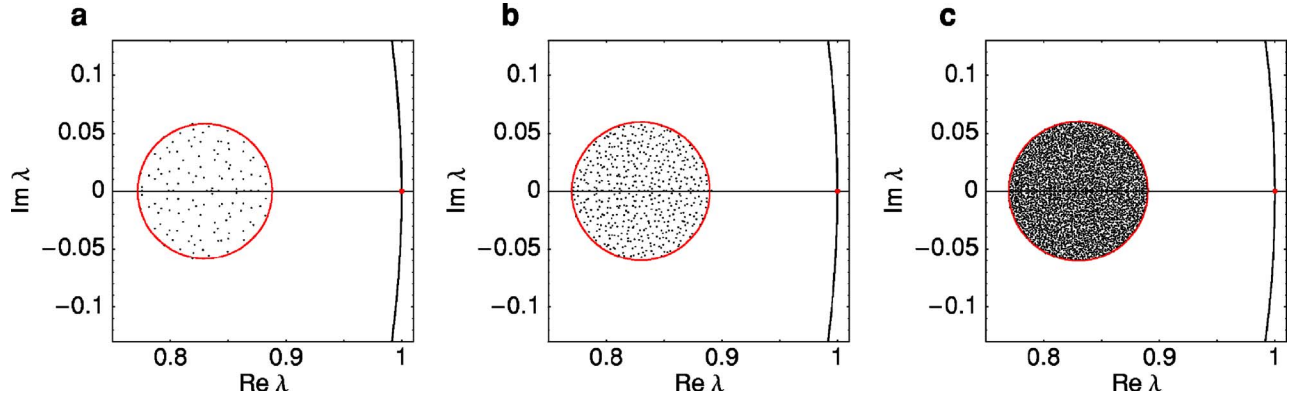


FIG. 6. Distribution of eigenvalues in the complex plane for networks with fixed in-degree $k=8$ for different network sizes (a) $N=128$, (b) $N=512$, (c) $N=4096$. The disks are centered at A_0 and have radius r_{RMT} , the prediction obtained from Random Matrix Theory. The arc through the trivial eigenvalue $z = \lambda_1 = 1$ is a sector of the unit circle. Parameters of integrate-and-fire oscillators are $I=1.1$, $\varepsilon=-0.2$, $\tau=0.05$.

probability p , the variance (83) is only an approximation because we replaced $[k_i^{-1}]_i$ by k^{-1} which gives the order of magnitude of the number of connections as a function of N .

Substituting $A_0 = 1 - \sum_{j \neq i} A_{ij}$ for integrate and fire neurons (57) into the radius prediction r_{RMT} , Eq. (85), we obtain

$$r_{\text{RMT}}^{\text{IF}} = \left(\frac{\varepsilon}{I e^{-\tau I_{\text{IF}}} - \varepsilon} \right) \left(\frac{1}{k} - \frac{1}{N} \right)^{1/2} \quad (86)$$

which explicitly contains all parameters of the system.

IX. NUMERICAL TESTS OF EIGENVALUE PREDICTIONS

We verified this scaling law for different parameters A_0 determined by different I , ε , and τ and found good agreement with numerically determined eigenvalue distributions. We compared the theoretical prediction (85) to the numerical data for both ensembles considered in Sec. VII.

A. Networks with constant in-degree

At a given network connectivity and given parameters, we obtained all eigenvalues of the stability matrix A for several network sizes N and in-degrees k . We find that the prediction obtained from Random Matrix Theory well describes the numerically determined eigenvalues. Examples of eigenvalue distributions for matrices at fixed k and three different N are shown in Fig. 6.

There are several ways to numerically estimate the radius of the disk of eigenvalues. For illustration, we use three different estimators here. The real part estimator

$$r_{\text{Re}} := \frac{1}{2} \left(\max_{i \neq 1} \text{Re}(\lambda_i) - \min_{i \neq 1} \text{Re}(\lambda_i) \right) \quad (87)$$

estimates the radius from the maximum spread of eigenvalues parallel to the real axis. Typically, r_{Re} should give an estimate that is too low compared to the radius obtained from the eigenvalues of an ensemble of matrices because it measures the maximal spread in one direction only. This is circumvented by the radial estimator

$$r_{\text{rad}} := \max_{i \neq 1} |\lambda_i - [A_0 - (1 - A_0)N^{-1}]| \quad (88)$$

that finds the maximum distance of any nontrivial eigenvalues from the average of the nontrivial eigenvalues, $\langle \lambda_i \rangle_{i \neq 1} = A_0 - (1 - A_0)N^{-1} + \mathcal{O}(N^{-2})$. This estimator should yield an approximation that may be too large compared to the respective ensemble average. The average estimator

$$r_{\text{av}} := \frac{3}{2} \frac{1}{N-1} \sum_{i=2}^N |\lambda_i - [A_0 - (1 - A_0)N^{-1}]| \quad (89)$$

estimates the radius r of a disk from the average distance $\langle d \rangle$ of eigenvalues from its center, because

$$\langle d \rangle = \int_0^{2\pi} \int_0^r r'^2 \rho(r') dr d\varphi = \frac{2}{3} r \quad (90)$$

if we assume a uniform $\rho(r') = 1/(\pi r^2)$ for $r' < r$ and $\rho(r') = 0$ otherwise (68). This estimate has the advantage, that it contains information from all eigenvalues in contradistinction to the two other estimators. Its disadvantage is that one has to assume *a priori* a uniform distribution of nontrivial eigenvalues. As displayed in Fig. 7, all three estimators converge towards the radius predicted by the random matrix model for large N and given in-degree k . Varying the in-degree k at fixed N also yields excellent agreement between the numerical data and the theoretical predictions for sufficiently large N and k . An example is displayed in Fig. 8.

For both, networks of fixed k and networks of fixed p , there are deviations for small and even for intermediate N , because the prediction r_{RMT} was obtained from Random Matrix Theory that is exact only in the limit $N \rightarrow \infty$, and the finite-size scaling of r_{RMT} was assumed to resemble the scaling of the variance of finite matrices. Furthermore, as discussed above, the numerical estimators of the radius rely on assumptions that are fulfilled only approximately. For sufficiently large networks, however, the theoretical prediction agrees well with the numerical data.

Thus there is a gap of size

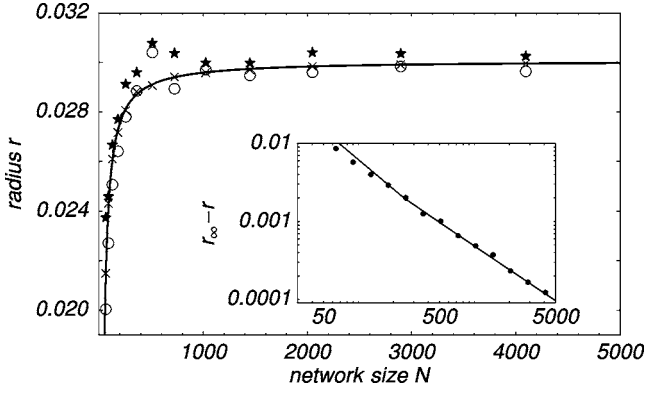


FIG. 7. Scaling of the radius r of the disk of nontrivial eigenvalues with the network size N at fixed in-degree $k=32$ ($I=1.1$, $\varepsilon=-0.2$, $\tau=0.05$). Main panel displays the radius r as a function of network size N . Symbols display r_{rad} (\star), r_{av} (\times), and r_{Re} (\circ). Inset displays $r_{\infty}-r$ as a function of N on a doubly logarithmic scale, where $r_{\infty}=(1-A_0)k^{-1/2}$. Dots display numerical data of r_{av} . In the main panel and the inset, lines are the theoretical prediction $r_{\text{RMT}}=(1-A_0)(1/k-1/N)^{1/2}$.

$$g = 1 - A_0 - r_{\infty} \quad (91)$$

between the nontrivial eigenvalues for large networks and the unit circle, where

$$r_{\infty} := \lim_{N \rightarrow \infty} r_{\text{RMT}} = (1 - A_0)k^{-1/2}. \quad (92)$$

This indicates that the stability of the synchronous state in the model system considered is robust, i.e., sufficiently small perturbations to the systems dynamics will not alter the stability results.

Nevertheless, there is an important restriction to these results. Given a fixed in-degree k , the limit $N \rightarrow \infty$ is not described by the theory derived in the preceding section, because the structure of the network considered and thus the structure of the stability matrices is only well defined if the network is connected in the sense that every oscillator has at least one presynaptic oscillator. However, the probability that at least one oscillator is disconnected from the remaining network approaches one with increasing network size. Thus

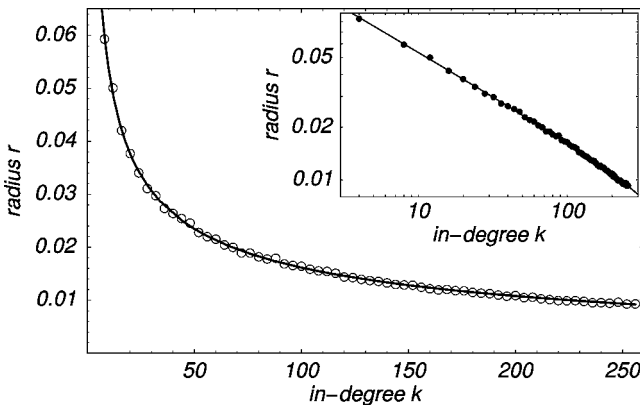


FIG. 8. Scaling of the radius r of the disk of nontrivial eigenvalues with the in-degree k for random networks of $N=1024$ oscillators ($I=1.1$, $\varepsilon=-0.2$, $\tau=0.05$). Main panel displays the radius r as a function of in-degree k . Inset displays the same data on a doubly logarithmic scale. Symbols display numerical results, using the average estimator r_{av} , lines are the theoretical prediction $r_{\text{RMT}}=(1-A_0)(1/k-1/N)^{1/2}$.

eigenvalue predictions of stability matrices of networks with fixed in-degree k are only reasonably described for network sizes that are large, $N \gg 1$, but not in the limit $N \rightarrow \infty$.

B. Networks with constant connection probability

If we assume that every connection is present with a constant probability p , the network will be connected with probability one in the limit $N \rightarrow \infty$ because the number of presynaptic oscillators k_i follows a binomial distribution with average pN and standard deviation $[p(1-p)N]^{1/2}$. In this limit, the radius of the disk of eigenvalues decreases with increasing network size N , see Fig. 9.

In order to verify the scaling behavior of the radius of the eigenvalue disk for large stability matrices A , we numerically determined the eigenvalues $\lambda_m = \max\{|\lambda_i| : |\lambda_i| < 1\}$, see Eq. (59), that are second largest in absolute value. For sufficiently large N , the theoretical prediction $\lambda_m \approx A_0 + r_{\text{RMT}}$ agrees well with the numerical data (Fig. 10). The radius approaches zero for large networks such that the eigenvalue second largest in absolute value converges towards the center A_0 of the disk. In conclusion, for large networks, all nontrivial eigenvalues are located near A_0 and are thus bounded away from the unit circle. This implies that the speed of synchronization that is determined by λ_m increases with increasing network size. Moreover, the condition necessary for robustness against structural perturbations of the systems dynamics is satisfied.

X. SYNCHRONIZATION SPEED AND SPEED LIMIT

The existence of bounds on the radius of the eigenvalue distribution has severe consequences for the synchronization speed of networks of neural oscillators. Whereas the largest (trivial) eigenvalue $\lambda_1=1$ corresponds to the invariant nature of the synchronized periodic orbit, the second largest eigenvalue λ_m [Eq. (59)] determines the asymptotic speed of synchronization starting from sufficiently close-by initial conditions. Because the dynamics can locally be approximated by a linear map, the synchronization of spike times is an exponential. Thus, denoting $\delta'(t) := \delta(t) - \lim_{s \rightarrow \infty} \delta(s)$, the distance $\Delta(n) := \max_i |\delta'_i(nT)| / \max_i |\delta'_i(0)|$ from the invariant state behaves as

$$\Delta(n) \sim \exp(-n/\tau_{\text{syn}}) \quad (93)$$

defining a synchronization time τ_{syn} in units of the collective period T . The speed of synchronization τ_{syn}^{-1} strongly depends on the parameters. For instance, as might be expected, synchronization is faster for stronger coupling.

Given the results from Random Matrix Theory derived above, we can deduce an expression for the synchronization time

$$\begin{aligned} \tau_{\text{syn}} &= -1/\ln(\lambda_m) \\ &= -1/\ln(A_0 + r_{\text{RMT}}) \end{aligned} \quad (94)$$

from the prediction of the second largest eigenvalue $\lambda_m \approx A_0 + r_{\text{RMT}}$. In general, upon increasing the coupling strength ε , the center A_0 of the disks of eigenvalues is moved towards zero, as can be seen from the defining equation (27). This means that, as expected, stronger interaction strengths

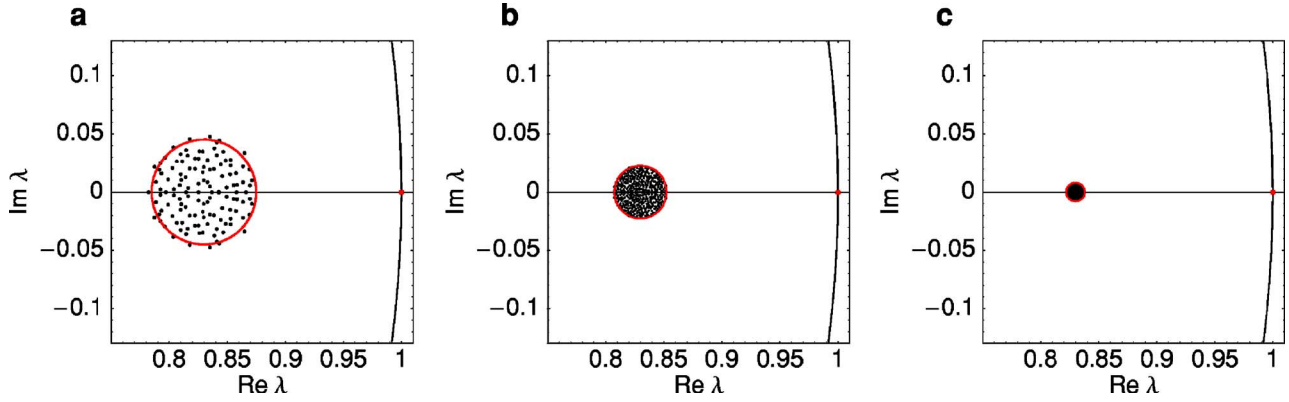


FIG. 9. Distribution of eigenvalues in the complex plane for networks with fixed connection probability $p=0.1$ for different network sizes (a) $N=128$, (b) $N=512$, (c) $N=4096$. The disks are centered at A_0 and have radius r_{RMT} , the prediction obtained from Random Matrix Theory. Note that the disk of nontrivial eigenvalues shrinks towards the point A_0 in the limit $N \rightarrow \infty$. The arc through the trivial eigenvalue $z=\lambda_1=1$ is a sector of the unit circle. Parameters of integrate-and-fire oscillators are $I=1.1$, $\varepsilon=-0.2$, $\tau=0.05$.

lead to faster synchronization of the spiking activity if all other dynamical parameters and the network are kept fixed. There is, however, a speed limit to synchronization if the in-degree of the network is finite. The speed limit plays a noticeable role if the typical in-degree k is significantly smaller than the number N of oscillators in the network.

For networks with constant in-degree (Fig. 11), the radius of the eigenvalue disk converges to a positive constant with increasing network size N . This means that the second largest eigenvalue does not converge to zero as the coupling increases arbitrarily strong. Thus the asymptotic synchronization time (94) is bounded below by

$$\tau_{\text{syn}}^{\varepsilon \rightarrow \infty} = \frac{2}{\ln k} \left(1 - \frac{k}{N \ln(k)} + \mathcal{O}(N^{-2}) \right) \quad (95)$$

for large N and thus limited by the network connectivity (cf. the asymptotes in Fig. 11).

For networks with fixed connection probability p , the radius of the eigenvalue disk does converge to zero with increasing network size N . However, for any finite network

with finite number of connections per oscillator, it has a positive radius and again leads to a speed limit, see Fig. 11. Note that in the example displayed the typical number of connections per oscillator is as large as $k \approx pN \approx 409$ but the speed limit is still prevalent.

Can we intuitively understand the speed limit that is enforced by the topology of the network, parametrized by its typical in-degree? Consider a large number of neural oscil-

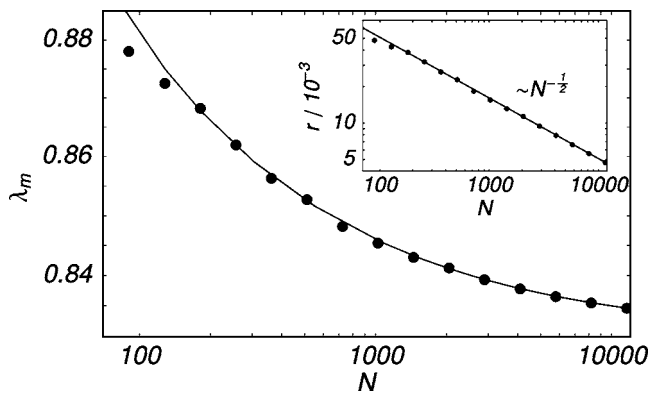


FIG. 10. Maximum nontrivial eigenvalue and the radius of the eigenvalue distribution for random networks (same parameters as in Fig. 9). Main panel displays the maximal nontrivial eigenvalue $\lambda_m \approx A_0 + r$ as a function of network size N . The maximal nontrivial eigenvalue converges to $A_0 \approx 0.83$ as $N \rightarrow \infty$. Inset displays the radius r of the disk of eigenvalues as a function of N . Dots display numerical results based on $r=r_{\text{rad}}$ [Eq. (88)], lines are the theoretical predictions for both, the radius r and the maximal nontrivial eigenvalue λ_m .

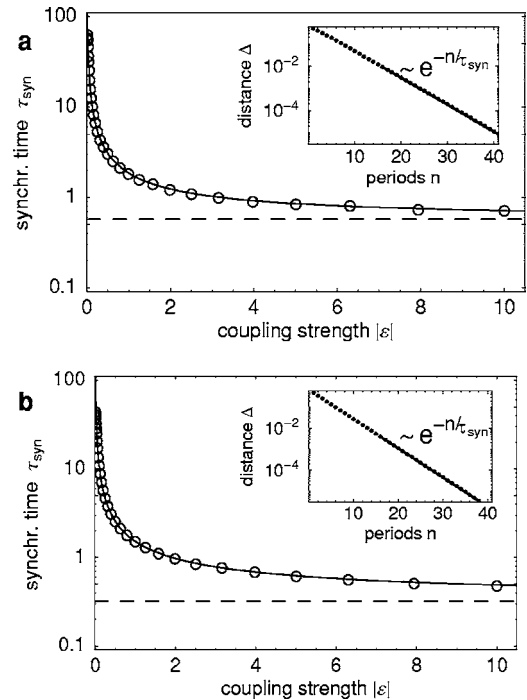


FIG. 11. Asymptotic synchronization time in random networks. (a) Network with fixed in-degree $k_i = k = 32$ [$N=1024$, $I=1.1$, $\tau=0.05$, $\varepsilon_{ij} = \varepsilon/k$ for $j \in \text{Post}(i)$]. Panel modified from Ref. 16. The inset shows the distance Δ of a perturbation δ from the synchronous state versus the number of periods n ($\varepsilon=-0.4$). Its slope yields the synchronization time τ_{syn} shown in the main panel as a function of coupling strength $|\varepsilon|$. Simulation data (○), theoretical prediction (—) derived in this paper, its infinite coupling strength asymptote (---). (b) Network of $N=2048$ neural oscillators and connection probability $p=0.2$. Other parameters and inset as in (a). Note that although the typical in-degree is changed drastically from (a) to (b), the synchronization speed limit is hardly affected.

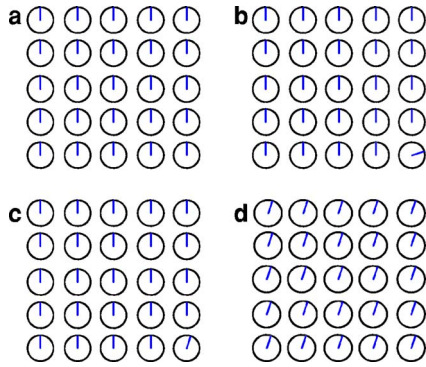


FIG. 12. Schematic illustrating the mechanism of resynchronization in a network of pulse-coupled neural oscillators. A collection of oscillators (connections not shown) at specific phases illustrated as “time on the clocks.” (a) Unperturbed, fully synchronous state. (b) One oscillator perturbed (out of phase). (c) Purely local restoring of phases might seem to be the natural way for resynchronization but it is not possible because local averaging of phases implies spreading of the perturbation such that finally (d) all oscillators of the network agree on a common phase that does not equal their original one.

lators connected via a network of complicated topology. If from the fully synchronous state [Fig. 12(a)] only one oscillator is perturbed away [Fig. 12(b)] this constitutes a simple example of resynchronization. One might imagine that all the other oscillators are pulling the phase of the perturbed one back to their common phase [Fig. 12(c)]. This would explain why, with increasing coupling strengths, synchronization would be faster—the stronger the local pulling force, the faster the local resynchronization. If that was the only mechanism involved, the network could be resynchronized arbitrarily fast using sufficiently large coupling strengths. The actual mechanism, however, is nonlocal. Because in the linearized dynamics each neural oscillator performs local averaging, see Eqs. (22)–(28), of their own phase and those phases of its presynaptic oscillators, the common phase of the resynchronized state will be globally agreed on [Fig. 12(d)], i.e., determined by the phases of all oscillators in the network. Neural oscillators can only interact with their neighbors, and, due to their pulsed interactions, only at discrete times once a period. For inhibitory interactions this means that the time between communication events is bounded below by $\Delta t_{\text{interact}} \geq 1$, independent of the delay time τ . At long times, the averaging must be performed all over the network, thus limiting the speed of synchronization.

XI. CONCLUSION

We have investigated the dynamics of synchronization in networks of neural oscillators with complex connection topology. We first described the stability analysis for the general case and found that the arising nonlinear and first order mappings have multiple state dependent parts. As an important consequence standard eigenvalue analysis of the first order system is not suitable. Using alternative methods, we demonstrated that the simplest periodic state, the synchronous state in which all neurons fire periodically at identical times, is stable for inhibitory coupling, independent of the specific network topology. Second, to study the speed of synchronization, we derived a subclass of models for which all

parts of the first order stability operators become degenerate. This class in general requires rise functions of integrate-and-fire type. Subsequently, we used Random Matrix Theory to analytically predict the speed of synchronization via the eigenvalue distributions depending on dynamical and network parameters. Numerical estimates are in excellent agreement with our theoretical predictions.

Although the theory used is based on Gaussian (i.e., fully occupied) matrices in the limit $N \rightarrow \infty$, our results also hold for sparse random networks with moderately large finite N . Moreover, it is known that the eigenvalue distribution of the sparse *symmetric* random matrix ensemble converges towards the eigenvalue distribution of the Gaussian symmetric ensemble in the limit $k \rightarrow \infty$. It is not clear whether a similar relation holds for Gaussian and sparse *asymmetric* ensembles as well. In fact it is an open question why the Gaussian ensemble actually describes the synchronization of sparse random networks even for small $k \approx 10^1$ rather than only for $k \rightarrow \infty$.

Our results also indicate that stable synchrony is common to a class of neural oscillators and not restricted to the specific model considered here. Moreover, given the expression for the speed of synchronization, we discovered a speed limit to synchronization on networks that is controlled by the typical in-degree of each oscillator, i.e., the number of other oscillators it receives input from. The dependence of the speed limit on the in-degree is logarithmic such that even for large in-degree the speed limit is significant.

The application of Random Matrix Theory in the present study suggests that it might well be possible to analytically predict dynamical properties of other systems from their structure, using an ansatz comparable to ours. Examples of the application of Random Matrix Theory in ecology are provided in Refs. 35 and 36. They were restricted to the dynamics near fixed points. Due to the idealization in the model class considered here, it was possible to analytically predict dynamical aspects near invariant (periodic) solutions that are not simple fixed points using Random Matrix Theory.

Some straightforward generalizations of possible application include less simple periodic states like cluster periodic orbits^{4,10,17} or periodic patterns of spikes which occur in the presence of heterogeneity.^{19,37–39} More interesting, and certainly more involved possibilities for Random Matrix Theory applications may arise if the dynamics becomes unstable. Of particular interest for theoretical neuroscience may be saddle periodic orbits which imply a high degree of flexibility when switching between states.^{10,40–44} Starting from the class of systems considered in the current paper, the next step into this direction would be to consider orbits that arise in networks where inhibitory and excitatory recurrent interactions coexist.^{5–7}

Our approach is not restricted to the well-known Erdős Renyi random graphs considered here. If other network topologies have to be considered, we expect that under some additional assumptions, just the associated random matrix ensemble could be used to describe the linearized dynamics of such systems. For future investigations of synchronization properties of networks, scale free and small world^{45,46} to-

pologies constitute promising candidates because these networks might be analytically tractable but nevertheless appear to reflect important aspects of real world networks.

ACKNOWLEDGMENTS

The authors thank Michael Denker, Tsampikos Kottos, Peter Müller, Haim Sompolinsky, Martin Weigt, and Annette Zippelius for useful discussions and comments on this work. This work was supported in part by the Federal Ministry of Education and Research (BMBF), Germany, under Grant No. 01GQ0430 (Bernstein Center for Computational Neuroscience BCCN Göttingen, Project A2).

- ¹F. Rieke, D. Warland, and W. Bialek, *Spikes: Exploring the Neural Code* (MIT Press, Cambridge, MA, 1999).
- ²P. Bressloff, S. Coombes, and B. de Souza, *Phys. Rev. Lett.* **79**, 2791 (1997).
- ³C. van Vreeswijk, L. F. Abbott, and G. B. Ermentrout, *J. Comput. Neurosci.* **1**, 313 (1994).
- ⁴U. Ernst, K. Pawelzik, and T. Geisel, *Phys. Rev. Lett.* **74**, 1570 (1995).
- ⁵C. van Vreeswijk and H. Sompolinsky, *Science* **274**, 1724 (1996).
- ⁶C. van Vreeswijk and H. Sompolinsky, *Neural Comput.* **10**, 1321 (1998).
- ⁷N. Brunel and V. Hakim, *Neural Comput.* **11**, 1621 (1999).
- ⁸C. van Vreeswijk, *Phys. Rev. Lett.* **84**, 5110 (2000).
- ⁹D. Hansel and G. Mato, *Phys. Rev. Lett.* **86**, 4175 (2001).
- ¹⁰M. Timme, F. Wolf, and T. Geisel, *Phys. Rev. Lett.* **89**, 154105 (2002).
- ¹¹N. B. A. Roxin and D. Hansel, *Phys. Rev. Lett.* **94**, 238103 (2005).
- ¹²R. E. Mirollo and S. H. Strogatz, *SIAM J. Appl. Math.* **50**, 1645 (1990).
- ¹³U. Ernst, K. Pawelzik, and T. Geisel, *Phys. Rev. E* **57**, 2150 (1998).
- ¹⁴W. Senn and R. Urbanczik, *SIAM J. Appl. Math.* **61**, 1143 (2001).
- ¹⁵M. Timme, F. Wolf, and T. Geisel, *Phys. Rev. Lett.* **89**, 258701 (2002).
- ¹⁶M. Timme, F. Wolf, and T. Geisel, *Phys. Rev. Lett.* **93**, 074101 (2004).
- ¹⁷M. Timme, F. Wolf, and T. Geisel, *Chaos* **13**, 377 (2003).
- ¹⁸M. Timme and F. Wolf (unpublished).
- ¹⁹M. Denker, M. Timme, M. Diesmann, F. Wolf, and T. Geisel, *Phys. Rev. Lett.* **92**, 074103 (2004).
- ²⁰G. Chartrand and L. Lesniak, *Graphs and Digraphs*, 3rd ed. (Chapman and Hall, Boca Raton, FL, 1996).
- ²¹M. Timme (unpublished).
- ²²E. P. Wigner, *Proc. Cambridge Philos. Soc.* **47**, 790 (1951).
- ²³*Statistical Theory of Spectra: Fluctuations*, edited by C. E. Porter (Academic, New York, 1965).
- ²⁴M. L. Mehta, *Random Matrices* (Academic, New York, 1991).
- ²⁵T. Guhr, A. Müller-Groeling, and H. A. Weidenmüller, *Phys. Rep.* **4–6**, 189 (1998).
- ²⁶O. Bohigas, M. J. Giannoni, and C. Schmit, *Phys. Rep.* **52**, 1 (1984).
- ²⁷F. Haake, *Quantum Signatures of Chaos* (Springer, New York, 2001).
- ²⁸D. A. Stariolo, E. M. F. Curado, and F. A. Tamarit, *J. Phys. A* **29**, 4733 (1996).
- ²⁹A. D. Mirlin and Y. V. Fyodorov, *J. Phys. A* **24**, 2273 (1991).
- ³⁰Y. V. Fyodorov and A. D. Mirlin, *Phys. Rev. Lett.* **67**, 2049 (1991).
- ³¹A. J. Bray and G. J. Rodgers, *Phys. Rev. B* **38**, 11461 (1988).
- ³²G. J. Rodgers and A. J. Bray, *Phys. Rev. B* **37**, 3557 (1988).
- ³³V. L. Girko, *Theor. Probab. Appl.* **29**, 694 (1985).
- ³⁴H. Sommers, A. Crisanti, H. Sompolinsky, and Y. Stein, *Phys. Rev. Lett.* **60**, 1895 (1988).
- ³⁵R. M. May, *Nature (London)* **261**, 459 (1976).
- ³⁶V. K. Jirsa and M. Ding, *Phys. Rev. Lett.* **93**, 070602 (2004).
- ³⁷D. Z. Jin, *Phys. Rev. Lett.* **89**, 208102 (2002).
- ³⁸C. Börgers and N. Kopell, *Neural Comput.* **15**, 509 (2003).
- ³⁹R.-M. Memmesheimer and M. Timme, e-print q-bio.NC/0601003 (2006).
- ⁴⁰D. Hansel, G. Mato, and C. Meunier, *Phys. Rev. E* **48**, 3470 (1993).
- ⁴¹M. Rabinovich, A. Volkovskii, P. Lecanda, R. Huerta, H. D. I. Abarbanel, and G. Laurent, *Phys. Rev. Lett.* **87**, 068102 (2001).
- ⁴²A. Zumdick, M. Timme, T. Geisel, and F. Wolf, *Phys. Rev. Lett.* **93**, 244103 (2004).
- ⁴³P. Ashwin and M. Timme, *Nonlinearity* **18**, 2035 (2005).
- ⁴⁴P. Ashwin and M. Timme, *Nature (London)* **436**, 36 (2005).
- ⁴⁵R. Monasson, *Eur. Phys. J. B* **12**, 555 (1999).
- ⁴⁶T. J. Farkas, I. Derényi, A. -L. Barabási, and T. Vicsek, *Phys. Rev. E* **64**, 026704 (2001).